Environmental Pollution 294 (2022) 118657

Contents lists available at ScienceDirect

Environmental Pollution

journal homepage: www.elsevier.com/locate/envpol

Inorganic and methylated mercury dynamics in estuarine water of a salt marsh in Massachusetts, USA☆

Ting Wang, Daniel Obrist *

Department of Environmental, Earth, and Atmospheric Sciences, University of Massachusetts Lowell, Lowell, MA, 01854, USA

ARTICLE INFO

Keywords:
New England coastal estuary
Mercury source
Vegetation uptake
Intertidal dynamic
Riverine export
Upper marsh

ABSTRACT

Salt marsh estuaries serve as sources and sinks for nutrients and elements to and from estuarine water, which enhances and alleviates watershed fluxes to the coastal ocean. We assessed sources and sinks of mercury in the intertidal Plum Island Sound estuary in Massachusetts, the largest salt marsh estuary of New England, using 25-km spatial water sampling transects. Across all seasons, dissolved (FHg) and total (THg) mercury concentrations in estuarine water were highest and strongly enhanced in upper marshes (1.31 ± 0.20 ng L^{-1} and 6.56 ± 3.70 ng L^{-1}, respectively), compared to riverine Hg concentrations (0.86 ± 0.17 ng L^{-1} and 0.88 ± 0.34 ng L^{-1}, respectively). Mercury concentrations declined from upper to lower marshes and were lowest in ocean water (0.38 ± 0.10 ng L^{-1} and 0.56 ± 0.25 ng L^{-1}, respectively). Conservative mixing models using river and ocean water as endmembers indicated that internal estuarine Hg sources strongly enhanced estuarine water Hg concentrations. For FHg, internal estuarine Hg contributions were estimated at 26 g yr^{-1} which enhanced Hg loads from riverine sources to the ocean by 44%. For THg, internal sources amounted to 251 g yr^{-1} and exceeded riverine sources six-fold. Proposed sources for internal estuarine mercury contributions include atmospheric deposition to the large estuarine surface area and sediment re-mobilization, although sediment Hg concentrations were low (average 23 ± 2 μg kg^{-1}) typical of uncontaminated sediments. Soil mercury concentrations under vegetation, however, were ten times higher (average 200 ± 225 μg kg^{-1}) than in intertidal sediments suggesting that high soil Hg accumulation might drive lateral export of Hg to the ocean. Spatial transects of methylated Hg (MeHg) showed no concentration enhancements in estuarine water and no indication of internal MeHg sources or formation. Initial mass balance considerations suggest that atmospheric deposition may either be in similar magnitude, or possibly exceed lateral tidal export which would be consistent with strong Hg accumulation observed in salt marsh soils sequestering Hg from current and past atmospheric deposition.

1. Introduction

Coastal areas account for about 4% of the total global land surface and are home to about 40% of the global population (UNEP, 2006). Among coastal wetlands, salt marshes are found in temperate and high latitudes (Mcowen et al., 2017) and represent one of the most productive and sensitive aquatic ecosystems with high species biodiversity (Gedan et al., 2009; Mcowen et al., 2017). Located between terrestrial and oceanic ecosystems, salt marshes provide many ecosystem services including preservation of water quality via filtration of storm water pollution, prevention of storm damage, and source and sink activity for nutrients and contaminants (Das et al., 2013; Lockfield et al., 2013; Marques et al., 2011; Pennings and Bertness, 2001). Due to increasing population pressures, salt marshes have been declining worldwide by 25%–50% between 1980 and 2005 (Crooks et al., 2011) and face numerous challenges such as negative impacts by urban sewage, industrial discharges, and agricultural and nutrient runoff (Mcowen et al., 2017).

The Plum Island Sound estuary in Massachusetts, USA is the largest salt marsh estuary in New England with a total surface area of 60 km^2, of which tidal wetland area account for 40 km^2 and open water area accounts for the remaining 20 km^2 (Hopkinson et al., 2018; Raymond and Hopkinson, 2003). Prior research shows that this salt marsh may be a hot spot of mercury (Hg) contamination – a neurotoxic global pollutant – as evident by enhanced Hg levels observed in blood of salt marsh sparrows, an important bird species endemic to salt marshes (Evers

☆ This paper has been recommended for acceptance by Bernd Nowack.

* Corresponding author.
E-mail addresses: Ting_wang@student.uml.edu (T. Wang), daniel_obrist@uml.edu (D. Obrist).

https://doi.org/10.1016/j.envpol.2021.118657
Received 21 May 2021; Received in revised form 6 November 2021; Accepted 6 December 2021
Available online 7 December 2021

et al., 2007; Lane et al., 2011). Blood Hg levels in salt marsh sparrows of the Plum Island Sound estuary exceeded a threshold limit of 1.2 ppm, a level shown to reduce nest success in wild songbird populations (Jackson et al., 2011), in 62% of sampled birds and were highest in comparison to levels found across other east coast estuaries (Lane et al., 2020). Proposed reasons for high biological Hg exposures in the Plum Island Sound salt marsh estuary include external sources such as riverine runoff and atmospheric deposition to the watershed (Lane et al., 2011; Evers et al., 2007; Driscoll et al., 2013). In addition to external sources, contents of Hg in salt marshes can be derived from internal sources such as sediment remobilization, channel erosion, and lateral tidal exchange between salt marshes and estuarine water during twice-daily tidal flooding, some of which may derive from legacy contamination sources (Seelen et al., 2020). In addition, Hg partitioning between filterable and solid phase Hg can result in deposition and accumulation in sediments, or alternatively mobilization of Hg from resuspension of sediments (Gilmour et al., 2018).

Salt marshes serve are inherent depositional environments for sediments which ultimately form the mineral component of soils and allow salt marshes to adapt dynamically to sea level fluctuations (Nixon, 1980). However, salt marshes also serve as sources for elements via lateral transfer from salt marshes to estuarine water and the nearby ocean (Schiebel et al., 2018; Tobias and Neubauer, 2009). In particular, salt marsh vegetation assimilates an excess of autochthonous carbon, which subsequently is mobilized via tidal exchanges to the coastal ocean, where, along with nutrients, it enhances ocean primary productivity (also termed "outwelling hypothesis") (Odum, 1980). Most salt marshes are considered net exporters of dissolved organic carbon (DOC) (Howes and Goehringer, 1994; Mitchell et al., 2012; Tzortziou et al., 2008). For Hg, only a few studies have provided insights on lateral transfer of Hg in salt marsh estuaries, and results indicate that they may serve both as sources and sinks of Hg depending on seasons and chemical species of Hg (Cesário et al., 2018, 2017b; 2016; Hung and Chmura, 2006; Mitchell et al., 2012; Weis and Weis, 2004).

A fraction of inorganic Hg is methylated to highly toxic monomethylmercury (MeHg) (Fitzgerald et al., 2007), which is the critical species leading to exposures to human and wildlife through consumption of fish and other aquatic organisms. In contrast to freshwater ecosystems where sediment production dominates as MeHg sources to water columns, MeHg in coastal wetlands may stem largely from watershed export or from MeHg formed in the offshore ocean where methylation occurs in sediments and the water column (Chen et al., 2014). Tidal marshes, however, also have been shown to be important locations for *in situ* MeHg production and accumulation (Canário et al., 2007; Cesário et al., 2017a; Gilmour et al., 2018; Lamborg et al., 2019) suggesting they contribute additional MeHg inputs to adjacent marine ecosystems (Langer et al., 2001; Fitzgerald et al., 2007; Mitchell et al., 2012; Zhang et al., 2014).

The objectives of this study were to quantify the spatial and temporal distribution of inorganic and methylated Hg in estuarine water across large transects in the Plum Island Sound salt marsh estuary and assess internal sources and sinks of Hg in comparison to external (i.e., watershed or ocean) sources and sinks. Sampling was performed along 25 km transects from the ocean through the salt marsh-dominated intertidal estuary to the main freshwater inlet of the Parker River. Water samples were collected across ten sampling locations during all four major seasons, and included both flood and ebb tidal cycle sampling. Additional seasonal sampling was conducted at four of the sampling locations to increase time resolution and extend sampling across two years (section 2.2). Water samples were analyzed for unfiltered total Hg (THg), filtered inorganic Hg (FHg), and filtered MeHg (FMeHg), along with auxiliary biogeochemical parameters such as total and dissolved organic carbon (TOC and DOC), sulfate (SO_4^{2-}), nitrate (NO_3^-), chloride (Cl^-), and sodium (Na^+). To assess internal estuarine Hg sinks and sources, we applied two-endmember mixing models using freshwater and ocean water endmembers with salinity as a conservatively mixed measure, whereby Hg concentrations in estuarine water that fall above the conservative mixing line indicates internal estuarine Hg sources while concentrations below the mixing line is indicative of estuarine Hg sinks (section 2.4).

2. Methods

2.1. Site description

The investigation was performed in the Plum Island Sound estuary on the northeastern coast of Massachusetts, USA at a latitude and longitude of 42°45′10″ and 70°56′46" (Fig. 1). The climate is northern temperate with an annual average precipitation of 1269 mm and mean monthly air temperatures of −4.4 °C in winter (January) to 21.8 °C in summer (July) based on the long-term records (1981–2010) at the nearest weather station (NOAA, Haverhill, MA, USA, USC00193505). River discharge of the Parker River watershed, which is the dominant tributary (Weinstein and Connors, 2001), averages from 2381 L s^{-1} in spring to a low of 500 L s^{-1} in fall (1946–2020) (USGS Water Data for the Nation, 2020) and is controlled by snow melt and higher precipitation in spring and low precipitation and high evapotranspiration and municipal water use in summer. The mean tidal amplitude at the Plum Island Sound estuary is 2.7 m (NOAA Tide Predictions, 2020). Salt marshes cover about 40 km^2 and account for 67% of the total estuary area (Hopkinson et al., 2018; Weinstein and Connors, 2001) and the rest of the area are open water surfaces (about 20 km^2) (Raymond and Hopkinson, 2003). Ratios of salt marsh to open water areas are as high as >10:1 in the upper marsh and about 1:1 in the lower marsh adjacent to the ocean (Hopkinson et al., 2018). In this study, we use the term upper marsh for sampling points dominated by river flow, lower marsh for sites located near the Plum Island Sound, and term sites in-between as middle marsh (Fig. 1). The dominant land covers of the Parker River watershed include forests (64.4%), urban areas (15.2%), wetlands (12.4%), agricultural land (4.7%), shrubs and grasslands (0.2%), and others (3.1%) (Scudder et al., 2009). Vegetation in the salt marsh is dominated by *Spartina patens*, *S. alterniflora, Distichlis spicata*, and *Juncus gerardii*, with *S. patens* dominating in high marshes and *S. alterniflora* dominating in low marshes. Salt marsh soils show a wide range of ages from 220 to 1614 years based on carbon dating of suspended particulate organic carbon and from 1800 to 3000 years based on organic carbon in the subsurface sediments (Hopkinson et al., 2018).

2.2. Water sampling

Water samples were collected by boat across 25-km transects with 10 sampling locations from the ocean (OW1 and OW2) through the intertidal area (TW1 to TW7) to the freshwater stream (denotes as PR for Parker River) four times between August 2019 and September 2020. At four sampling locations, additional water samples were collected bimonthly between October 2018 and July 2019 to delineate seasonal trends. We replicated sample collections at fresh water (PR) and ocean water sites (OW1 and OW2), but no replicate samples were taken in the estuary where we instead sampled twice during each sampling campaign to represent both ebb and flow tides. Water samples were collected using 125 mL and 500 mL acid-cleaned (10% hot hydrochloric acid [HCl]) Teflon bottles for Hg samples (THg, FHg, and FMeHg). Bottles were double bagged and preserved with 0.5% HCl before sampling. All samples were stored at 4 °C until analysis. For other water quality measures (e.g., TOC and DOC, SO_4^{2-}, NO_3^-, Cl^-, Na^+), samples were taken in 50 mL polypropylene Falcon® tubes (Corning, New York, USA). We used "clean hands/dirty hands" methods for water sampling based on the EPA method (USEPA, 2002), and sampling containers were rinsed three times with water samples before taking the final samples. Water samples were double bagged and kept in coolers on ice immediately after sample collection and were transported to the laboratory at UMass Lowell within 8 h. Half of the water samples were filtered (after

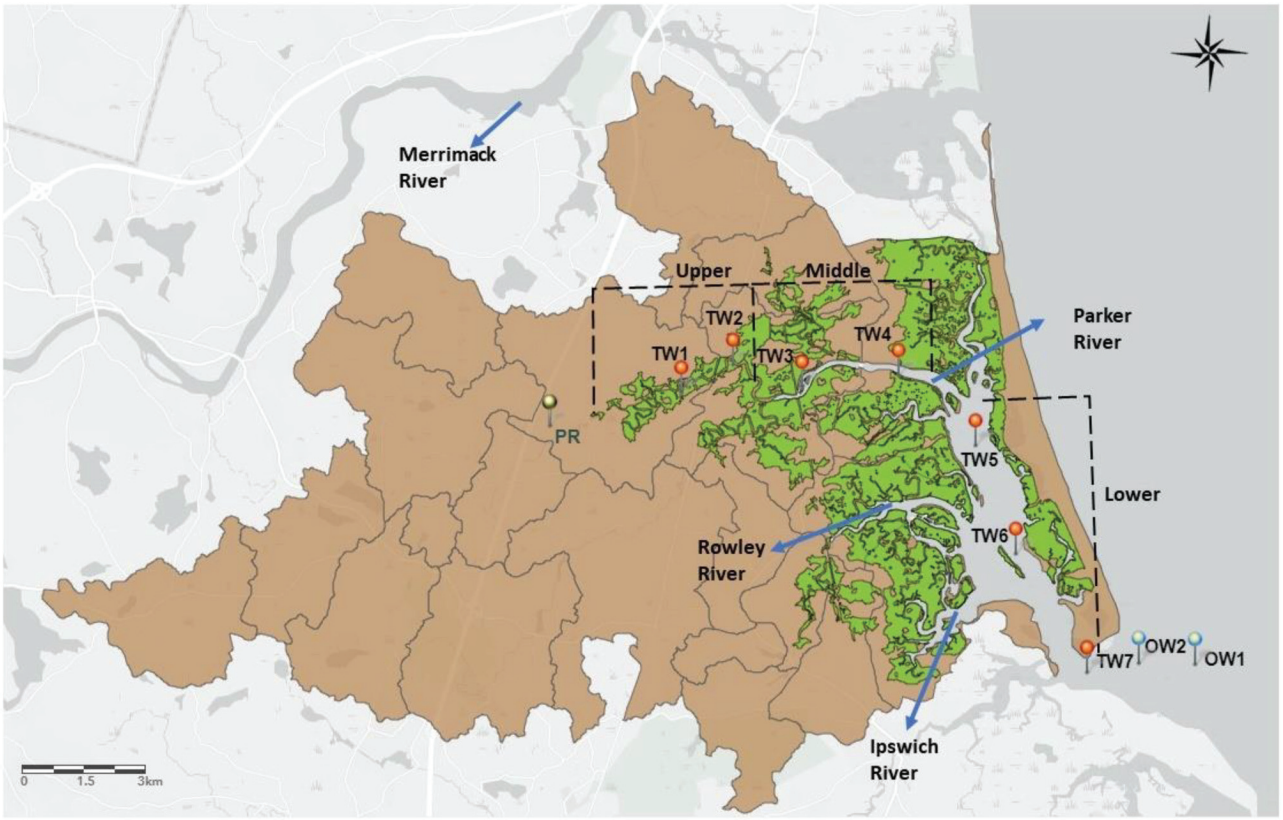

Fig. 1. Map of the Parker River watershed (brown colors) with an approximate size of 212 km^2, and the salt marsh estuary with about 20 km^2 of water surface and 40 km^2 of salt marsh cover (shown in green). Seven sampling sites for estuarine water samples are located in the tidal estuary (red pins). The green pin shows the location of the freshwater site (Parker River above the marsh) and blue pins are ocean water sampling sites. (For interpretation of the references to color in this figure legend, the reader is referred to the Web version of this article.)

thorough mixing) within 48 h of sample collection using 0.45 μm filters (Acrodisc 32 mm Syringe Filter with 0.45 μm Supor Membrane, Becton Dickinson, New Jersey, USA) and preserved with 0.5% HCl for dissolved Hg and MeHg analysis. Unfiltered samples were preserved with 0.5% HCl for THg analysis. All samples were stored at 4 °C until analysis. Laboratory blank tests were below the method detection limit and showed no detectable contamination from filtration and sampling containers.

2.3. Analytical methods

Total and dissolved Hg concentrations in water samples were measured in duplicates using a Tekran water analysis system (Model 2600 Water Analyzer, Tekran Inc., Toronto, Canada) using oxidation, purge, trap, desorption, and cold-vapor atomic fluorescence spectrometry (CVAFS) based on EPA method 1631, revision E (USEPA, 2002). 25 mL samples were digested with addition of 0.125 mL full-strength bromine mono-chloride (BrCl) overnight prior analysis. Prior to analysis, 0.03 mL of hydroxylamine hydrochloride (HH) was added to neutralize free halogens and 0.06 mL stannous chloride ($SnCl_2$) to reduce Hg species contained in water to gaseous Hg. Six-point calibration curves (concentrations of 0.0, 0.5, 1.0, 5.0 10, and 25 ng L^{-1}) were performed before every day of analysis. Quality control steps included at least three calibration blanks, ongoing precision recoveries (OPR) with concentrations of 5 ng L^{-1}, and matrix spike duplicates (MSD) with concentrations of 10 ng L^{-1} added after every ten samples. The analyzer detection limit, based on 3 times of the standard deviation of calibration blank samples, were estimated to be 0.03 ± 0.02 ng L^{-1}. Recoveries of OPR standards averaged 101.8 ± 6.5% and were always within 85–115%. Spike recoveries averaged 93.8 ± 14.7% and always were within a range of 77–111%. Laboratory blank tests were below the method detection limit and showed no detectable contamination from filtration and sampling containers.

Aqueous MeHg concentrations were measured in duplicates using a Tekran MeHg system (Model 2700, Tekran Inc.) with a fully-integrated gas chromatograph separation and cold vapor atomic fluorescence spectrometry (GC-CVAFS) following the technique described by Munson et al. (2014) modified based on EPA Method 1630 (USEPA, 2001). 28 mL samples were digested with 1% sulfuric acid (H_2SO_4) overnight to ensure the reaction time was at least 12 h prior to analysis. Potassium hydroxide (KOH), 0.75% acetate buffer (mixed with sodium acetate and glacial acetic acid in reagent water), 2.5% L-ascorbic acid (AA) and 0.1% sodium tetraethylborate were added to samples before analysis. Seven-point calibration curves (concentrations of 0.0, 0.02, 0.05, 0.1, 0.5, 1.0 and 2.0 ng L^{-1}) were done before every daily analysis. Quality control steps included three calibration blanks, ongoing precision recoveries (OPR) with concentration of 0.5 ng L^{-1}, and matrix spike and matrix spike duplicate (MSD) with concentration of 1.0 ng L^{-1} every ten samples. The analyzer detection limit, based on 3 times of the standard deviation of the reagent blanks, were estimated to be 0.013 ± 0.007 ng L^{-1}. Recoveries of standards averaged 95.7 ± 9.3% and spike recoveries averaged 96.8 ± 33.8%. Additionally, the high variability of spike recoveries is mainly due to large variability for the MeHg at very low concentrations in water samples.

Samples for the DOC analysis were filtered by 0.45 μm syringe filters and unfiltered water samples were used to measure TOC concentrations. Measurement were conducted using a Total Organic Carbon Analyzer (Model TOC-$L_{CPH/CPN}$, Shimadzu, Marlborough, Massachusetts, USA). Major element analyses on filtered samples included analysis of sodium (Na), calcium (Ca), magnesium (Mg) and potassium (K) measured with

inductively coupled plasma - optical emission spectrometry (ICP-OES) (Model 5100, Agilent, Santa Clara, California, USA) using 5-point calibration curves (concentrations of 0.0, 0.01, 0.1, 1.0 and 10 mg L^{-1}). Filtered water samples also were analyzed for major anions using an external laboratory (Soil, Water and Forage Analysis Laboratory at Oklahoma State University) whereby aqueous S was analyzed using a Spectro Arcos II ICP-OES and converted to SO_4–S as anion. NO_3^- was analyzed using a Lachat flow injection analyzer with the method of 10-107-04-1-A (Wendt, 2001), and Cl^- was analyzed with the same analyzer with NO_3^- but with different method, 10-117-07-1-B (Pruefer, 2007).

2.4. Data analysis

A two end-member mixing model was used to calculate conservative mixing of constituents between river inputs and ocean water and to quantify internal sources and sinks in comparison with external sources (Officer, 1979; Boyle et al., 1974). The approach has been applied in the Plum Island Sound salt marsh estuary for the study of particulate organic carbon (POC) dynamics (Hopkinson et al., 2018) and the Neponset River estuary nearby Boston for the study of DOC dynamics (Schiebel et al., 2018), and assumes steady state conditions. In short, Hg concentrations are plotted against salinity (e.g., chloride concentrations) with linear regressions showing conservative mixing between riverine (i.e., Parker River) and ocean water end-members. Data points in estuarine water samples that fall above or below conservative mixing lines are indicative of internal estuarine sources or sinks. Zero y-axis intercepts of the conservative regression lines denominate Freshwater Endmember (FEM) points, which in our case are equivalent to measured riverine water concentrations (Table 2). The y-axes intercepts of tangential fits of curvilinear curves in intertidal samples denote Apparent Endmember (AEM) concentrations indicative of internal sinks or sources. In our case, data of estuarine water samples best fit linear curves, which may be due to non-steady conditions or uneven source/sink distributions (see discussion). To be consistent, we consistently used linear fits to data which overall best fit measurements. We used linear regression models to test for statistical significances between conservative mixing lines (ocean and river water) and tidal water regression lines. Differences between FEM and AEM are used as estimates to quantify relative enhancement or decrease of concentrations due to internal sources or sinks in the salt marsh estuary. Note that salinity of ocean water samples were quite variable during some sampling periods indicating some dilution of ocean water samples with freshwater; however, the effect on the mixing lines were relatively minor so that we decided to keep all ocean samples in the dataset.

For other statistical tests, data were transformed by Johnson Transformation to achieve normal distributions. Statistical differences between flood and ebb tide samples were assessed by paired Student t-tests using both concentrations and Hg:chloride ratios. Statistical differences between river, ocean, and different estuarine sampling locations (i.e., upper, middle, and lower marsh) were tested via unpaired t-tests. Correlation matrices were used to assess relationships among Hg concentrations and major geochemical variables. All statistical tests were conducted using STATA (Version 16.0, Statacorps, College Station, Texas). All regressions and statistical tests presented in text, tables, and figures denote statistical differences at $p < 0.05$, unless noted otherwise.

3. Results

3.1. Transect patterns of inorganic total and filtered Hg

Across the four sampling dates, inorganic filtered Hg concentrations (FHg: 0.45 μm pore size filtering) showed highest concentrations (1.31 ± 0.20 ng L^{-1}) in estuarine water of the upper marsh (locations TW1 and TW2, 17 and 15 km upstream from the ocean, respectively). These concentrations were statistically higher than concentrations at all other locations, including those of the Parker river water (PR) which averaged 0.86 ± 0.17 ng L^{-1}. Concentrations were statistically lower in the middle marsh (locations TW3 to TW4, 12 and 10 km distances from ocean, respectively) where concentrations averaged 0.84 ± 0.20 ng L^{-1}. Concentrations further were statistically significantly lower in the lower tidal water closest to the ocean (locations TW5, TW6 and TW7, 7, 4, and 1 km distances from the ocean, respectively), where concentrations averaged 0.45 ± 0.17 ng L^{-1}. Concentrations were lowest in ocean water collected 1 and 2 km off the coast in open ocean water averaging 0.38 ± 0.10 ng L^{-1} (Table 1, Fig. 2). These patterns were similar across all four seasons (see section 3.3 for seasonal patterns). Differences in FHg between flood and ebb tides were not statistically significant overall and somewhat variable and inconsistent across the sampling seasons. For example, in August 2019 and February 2020, higher aqueous FHg concentrations were observed during flood tides compared to ebb tides, and reversed patterns were observed in May 2020 (Fig. 2). When Hg concentrations were standardizing for salinity, concentration differences between flood and ebb tide samples largely disappeared (Fig. 3) suggesting that differences in concentrations likely were related to sampling at different points of the tidal curve (see discussion 4.1).

Concentrations of unfiltered inorganic Hg (THg) were much higher compared to FHg due to contributions of particulate Hg. Patterns of THg (Fig. 2) generally were similar as FHg but showed much stronger Hg concentrations enhancements in the salt marsh estuary compared to both freshwater (average of 0.88 ± 0.34 ng L^{-1}) and ocean water (average of 0.56 ± 0.25 ng L^{-1}). Highest THg concentrations were measured in the upper marsh (average of 6.56 ± 3.70 ng L^{-1}) followed by the middle marsh (average of 4.08 ± 2.10 ng L^{-1}) and were lowest in the lower marsh (1.04 ± 0.74 ng L^{-1}) (Table 1), and all differences were statistically significant. THg concentrations were more variable than FHg concentrations, however, likely due to variable sediment and particulate organic carbon loads of samples (see below). In Parker River freshwater samples, more than 95% of aqueous Hg was in dissolved form, but only averaged 20% in the upper and middle marsh estuary. Filtered Hg contributions increased again to 44% in the lower marsh and to 68% in ocean water (Table 1). For THg, differences between flood and ebb tides also varied and concentrations in flood tide samples were statistically higher compared to ebb tide samples in two of the four sampling dates (i.e., August and May; Figs. 2 and 3).

Chloride is a conservative element that has no specific sources or sinks in the tidal estuary so that its concentration is determined by conservative mixing between river and ocean water (Officer, 1979). Fig. 3 shows FHg and THg concentrations graphed against chloride concentrations with blue regression lines representing conservative mixing lines between Parker River freshwater and ocean water end-members. Aqueous FHg concentrations in estuarine water were consistently above conservative mixing lines in all seasons, indicative of internal sources of Hg that cannot be explained by mixing of river and ocean water (Officer, 1979; Boyle et al., 1974). Such internal sources and sinks have been observed for iron in salt marsh estuaries (sinks; Boyle et al., 1974) and DOC (sources; Raymond and Hopkinson, 2003) and generally show curvilinear behaviors (e.g., convex patterns). In our study, estuarine Hg concentrations were best explained by linear fits (Fig. 3). With the exception of September 2020 (Fig. 3d), regression lines for estuarine water samples were statistically different from conservative mixing lines, with coefficients of determination, r^2, ranging from 69% to 98% for FHg (Fig. 3a to d). Similar regressions were observed between estuarine water THg and chloride concentrations, with statistically significant differences to the conservative mixing lines during the same three sampling dates. In agreement with generally higher variability of THg concentrations, coefficients of determinations, r^2, were lower for THg (ranging from 39% to 83%, Fig. 3e to h) than for FHg.

Tangential fits of the curvilinear patterns and respective y-axis intercepts (i.e., extrapolating data to zero salinity) are used to determine Apparent Endmember (AEM) concentrations, which are quantitative measures of estuarine internal source or sink strengths (Schiebel et al.,

Table 1
Summary of analytical results of averaged Hg and auxiliary parameters across various sampling locations in estuarine water of the Plum Island Sound salt marsh estuary.

Location	THg	std	FHg	std	%FHg[a]	MeHg	std	%MeHg[b]
	ng L^{-1}		ng L^{-1}			ng L^{-1}		
Fresh Water	0.88	0.34	0.86	0.17	97	0.200	0.137	23.3
Upper Marsh	6.56	3.70	1.31	0.20	20	0.102	0.042	7.7
Middle Marsh	4.08	2.10	0.84	0.20	21	0.068	0.040	8.0
Lower Marsh	1.04	0.74	0.45	0.17	44	0.045	0.038	9.8
Ocean Water	0.56	0.25	0.38	0.10	68	0.039	0.033	10.4

Location	DOC	std	TOC	std	Cl	std	SO_4–S	std	NO_3–N	Std
	mg L^{-1}		mg L^{-1}		mg L^{-1}		mg L^{-1}		mg L^{-1}	
Fresh Water	6.7	1.3	6.3	1.9	303	307	23	24	0.16	0.10
Upper Marsh	5.4	1.6	6.8	2.8	6507	5513	1030	815	0.12	0.11
Middle Marsh	3.7	0.9	3.8	0.9	11288	4235	1720	578	0.07	0.08
Lower Marsh	2.2	0.9	2.2	0.9	15382	2204	2206	236	0.10	0.09
Ocean Water	1.8	0.2	1.9	0.7	16180	2267	2196	231	0.07	0.07

[a] %FHg indicates ratioes between FHg and THg.
[b] %MeHg indicates the ratioes between MeHg and FHg.

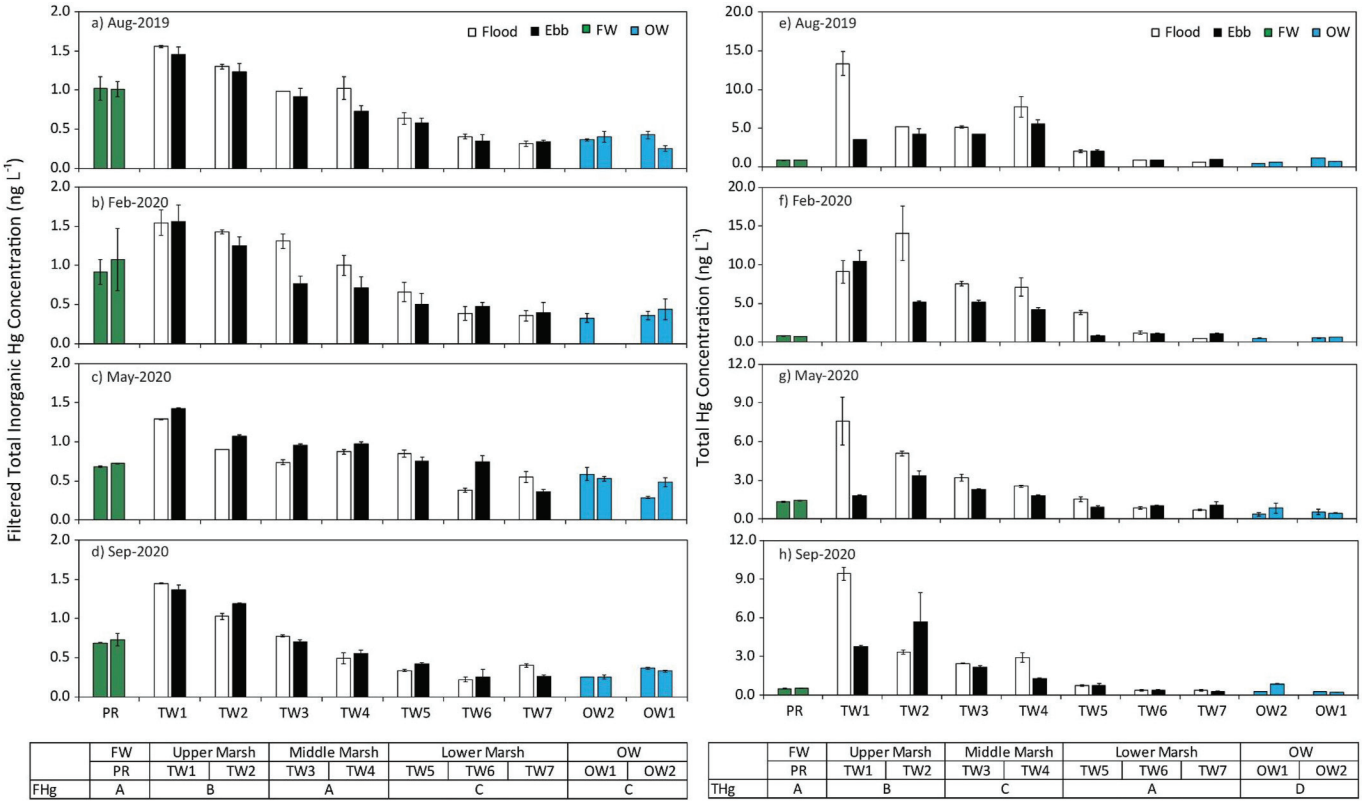

Fig. 2. FHg concentrations of water samples collected in a) Aug-2019, b) Feb-2020, c) May-2020, and d) Sep-2020. Total Hg (THg) concentrations of water samples collected in e) Aug-2019, f) Feb-2019, g) May-2020, and h) Sep-2020. PR (green bars) represents the fresh water site; OW2 and OW1 are ocean water sites (blue bars); all other sites are estuarine water sites, with black bars representing ebb tides and open bars representing flood tides. No statistic difference between flood and ebb tides (paired Student t-test, $p > 0.1$). Error bars indicate analytical replicates. Different letters in the table below indicate significant differences. (For interpretation of the references to color in this figure legend, the reader is referred to the Web version of this article.)

2018). Following this concept, we calculated y-axis intercepts of linear regression fits of estuarine water samples to estimate AEM for Hg (Table 2). Compared to conservative mixing line intercepts (which denote Freshwater Endmember: FEM), AEM concentrations of FHg in estuarine samples were enhanced by 1.2 ng L^{-1}, 0.5 ng L^{-1}, 0.6 ng L^{-1}, and 0.6 ng L^{-1} in August, February, May, and September, respectively. This corresponds to enhancements of 128%, 52%, 86%, and 81% of AEM concentrations relative to FEM concentrations (i.e., AEM/FEM x 100%; Table 2). Slopes and intercepts of THg were more strongly enhanced in estuarine water compared to the freshwater-ocean water mixing lines with relative concentration enhancements of AEM relative to FEM of 244 to 1929% (Table 2). These results support strong internal sources of THg within the salt marsh estuary, although uncertainty ranges of AEM were larger for THg due to higher variability.

3.2. Transect patterns of filtered organic MeHg

In contrast to FHg and THg, filtered methylmercury (FMeHg)

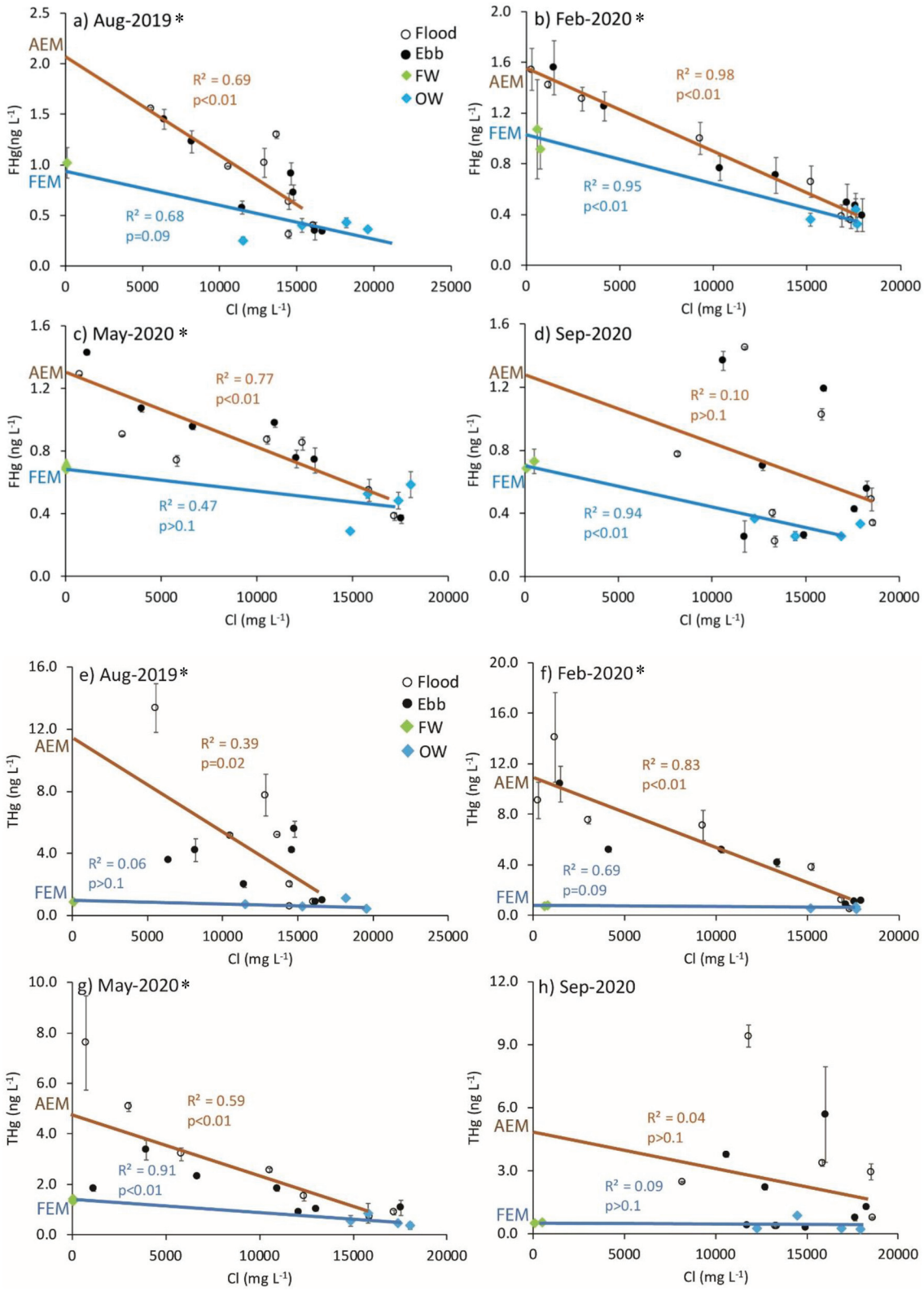

Fig. 3. FHg concentrations plotted against salinity (Cl concentrations) of samples collected in a) Aug-2019, b) Feb-2020, c) May-2020, and d) Sep-2020. Standardizing the THg concentrations by salinity (Cl concentrations) of waters collected in e) Aug-2019, f) Feb-2020, g) May-2020, and h) Sep-2020. Blue lines show conservative mixing lines between fresh and ocean water samples. Brown lines represent linear regression lines of estuarine water samples. Error bars indicate analytical replicates. FEM indicates freshwater member and AEM is the apparent end member concentration. Asterix shows when AEM concentration is statistically higher than FEM concentration based on linear regression analysis. (For interpretation of the references to color in this figure legend, the reader is referred to the Web version of this article.)

concentrations were highest in river water (average of 0.200 ± 0.137 ng L^{-1}), followed by statistically significantly lower concentrations in the upper marsh (average of 0.102 ± 0.042 ng L^{-1}) and middle marsh (average of 0.068 ± 0.040 ng L^{-1}). Lowest concentrations were observed in the lower marsh (average 0.045 ± 0.038 ng L^{-1}) which was not statistically different to ocean water concentrations (average 0.039 ± 0.033 ng L^{-1}) (Table 1, Fig. 4). FMeHg concentrations, however, were highly variable. Seasonally, concentrations were similar in February and May and lowest in September (Fig. 4). No statistical differences of FMeHg were observed between flood and ebb tide water samples across any of the sampling dates. Percent FMeHg (%MeHg) of total FHg was highest in river water (23.3%) and was statistically different to an average of 10.0% in the ocean and lower marsh, 7.7% in the upper marsh water, and 8.0% in the middle marsh (Table 1). These patterns were largely driven by respective inorganic FHg enhancements in estuarine water, as opposed to concentrations variations of FMeHg. In February and May, FMeHg concentrations of nearly all estuarine water samples fell below conservative mixing lines of river and ocean water samples while patterns were highly variable in September (Fig. 5). Similar to inorganic Hg, FMeHg concentrations in estuarine water best fit linear regression lines (as opposed curvilinear fits). Statistical test of regression lines showed estuarine water samples followed statistically lower regression slopes compared to conservative mixing lines in February and May 2020 (Table S1), indicative of FMeHg sinks, although the latter showed a very poor linear fit (Fig. 5).

3.3. Transect patterns of auxiliary biogeochemical parameters

In Figs. S1, S2, S3, S4 and Table 1, we show auxiliary biogeochemical parameters including DOC, TOC, Cl^-, SO_4^{2-} concentrations, and their respective patterns along the sampling transects. Spatial patterns of DOC showed highest average concentrations in Parker River freshwater (6.7 ± 1.3 mg L^{-1}), which were significantly higher than the average concentrations of other sites in upper, middle, and lower marshes (Fig. S1). Concentrations gradually and statistically significantly decreased from the upper marsh (average of 5.4 ± 1.6 mg L^{-1}) to the middle marsh (3.7 ± 0.9 mg L^{-1}) and the lower marsh (2.2 ± 0.9 mg L^{-1}). DOC concentrations were lowest in ocean water (average of 1.8 ± 0.2 mg L^{-1}) (Table 1). Similar transect patterns were observed for TOC concentrations (Table 1, Fig. S2), with the exception that TOC concentrations in the upper marsh estuarine water were not statistically significantly different to river water.

A correlation matrix of estuarine water samples (excluding ocean water and freshwater samples) showed strongest correlations among sea salt cations and anions (Cl. SO_4^{2-}, K, Ca, K, Mg, and Na) with correlation coefficients (r) generally above 0.95 (Table S3). FHg was most strongly correlated with THg (0.77), PHg (0.71), TOC (0.76), and DOC (0.68), and significant negative correlations were observed between FHg and dominant sea water cations and anions (−0.64 to −0.67). THg also showed strong correlations with TOC (0.63) and DOC (0.47), along with negative correlations to salinity parameters, although r values generally were lower (−0.39 to −0.44). For FMeHg, we found significant positive correlations with FHg (0.44), DOC (0.51), and TOC (0.47), and negative correlations with sea salts (−0.61 to −0.67). Assessing correlations between FHg and DOC more closely, significant linear correlations were observed across all estuarine water samples and sampling dates with coefficients of determination (r^2) ranging from 56% to 86% (Fig. S5). Using conservative mixing models as described above, we found that DOC-FHg correlations of estuarine water samples follow different slopes compared to that of freshwater and ocean samples and showed

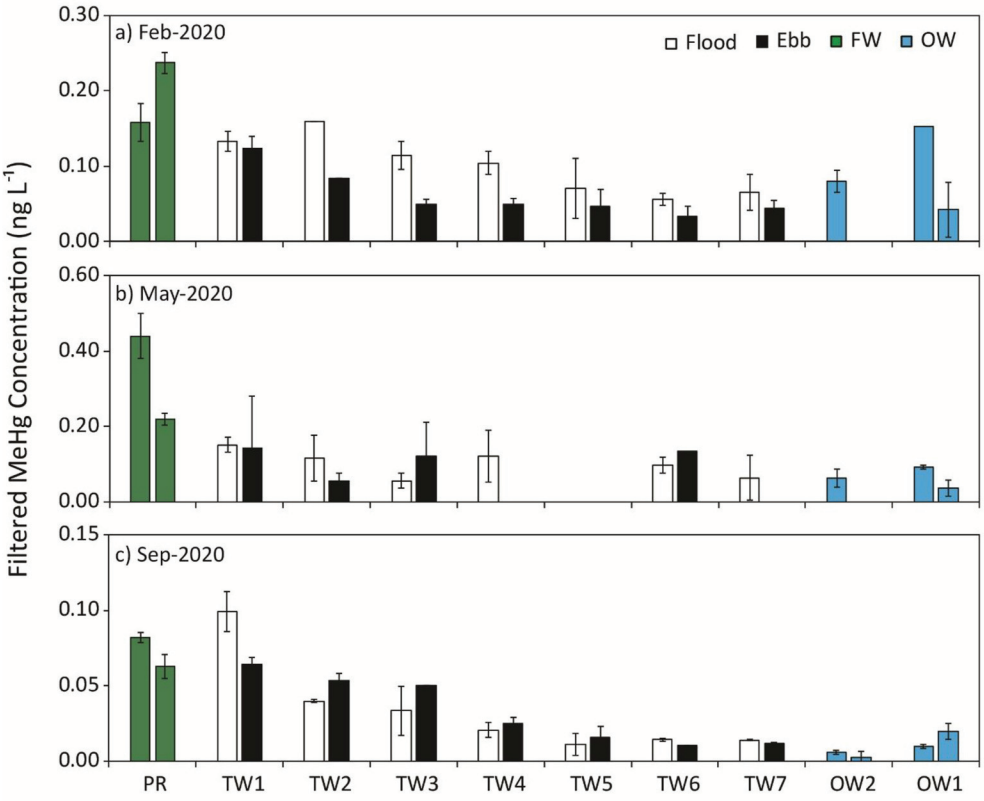

	FW	Upper Marsh		Middle Marsh		Lower Marsh			OW	
	PR	TW1	TW2	TW3	TW4	TW5	TW6	TW7	OW1	OW2
MeHg	A	B		C		C			C	

Fig. 4. Filtered MeHg concentrations of water samples collected in a) Feb-2019, b) May-2020, and c) Sep-2020. PR (green bars) represents the fresh water site; OW2 and OW1 are ocean water sites (blue bars); all other sites are estuarine water sites, with black bars representing ebb tides and open bars representing flood tides. No statistic difference between flood and ebb tides (paired Student t-test, $p > 0.1$). Error bars indicate analytical replicates. Different letters in the table below indicate significant differences. (For interpretation of the references to color in this figure legend, the reader is referred to the Web version of this article.)

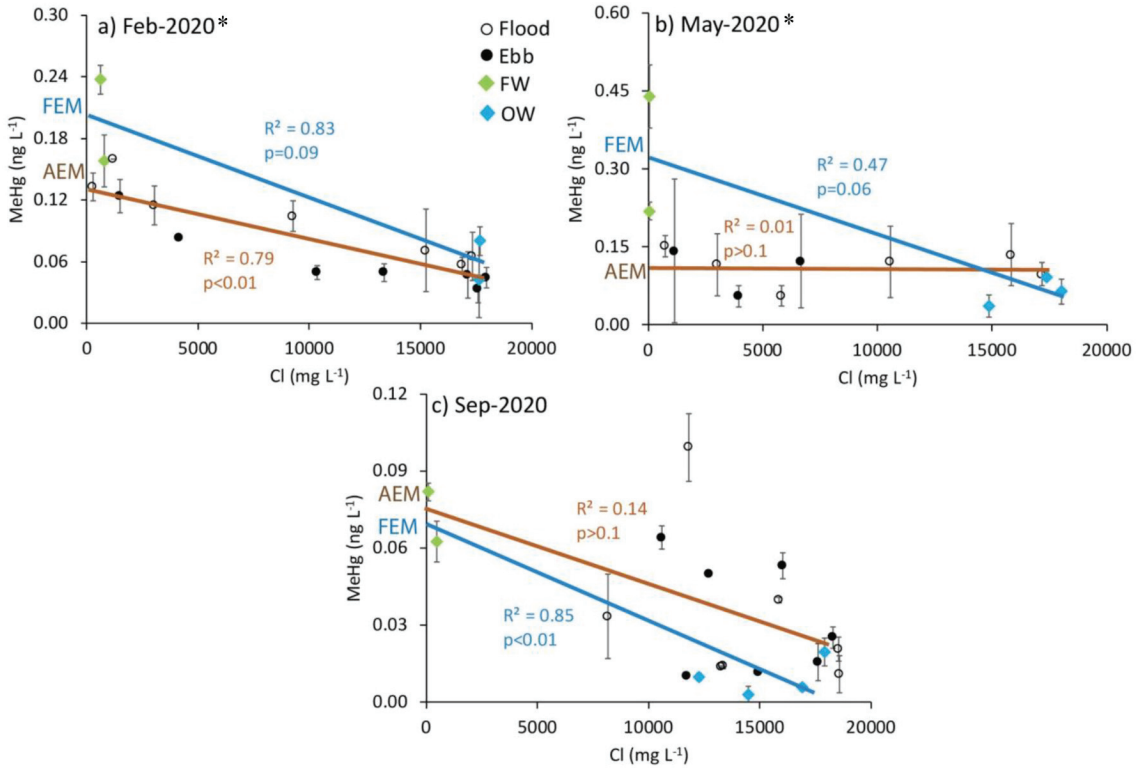

Fig. 5. FMeHg concentrations plotted against salinity (Cl concentrations) of water samples collected in a) Feb-2020, b) May-2020, and c) Sep-2020. Blue lines show conservative mixing lines between fresh and ocean water samples. Brown lines represent linear regression lines of estuarine water samples. Error bars indicate analytical replicates. FEM indicates freshwater member and AME is the apparent end member concentration. Asterix shows when AEM concentration is statistically higher than FEM concentration based on linear regression analysis. (For interpretation of the references to color in this figure legend, the reader is referred to the Web version of this article.)

consistently enhanced FHg to DOC ratios in estuarine water. Statistical tests showed that slopes of DOC concentrations in estuarine water were statistically enhanced in May and September 2020 compared to conservative freshwater-ocean water mixing lines, while no significant differences in slopes or intercepts were found for the two other dates in spite of some DOC enhancements (Fig. S5, Table S2). Furthermore, no statistical differences in correlations between FHg and DOC were observed between flood and ebb tide samples (Fig. S5). Linear regressions between TOC and THg in estuarine water showed patterns similar to those between DOC and FHg, but with lower coefficients of determination (from 40% to 74%) (Fig. S6, Table S2). Finally, FMeHg concentrations in estuarine water samples showed positive regressions with DOC in February and September, with coefficients of determination (r^2) of 65% and 69%, respectively, but no linear regression were bound for May 2020 when data were highly variable (2%) (Fig. S7). Statistical test showed slope in estuarine water were statistically different in May 2020, but not in other two sampling dates (Table S2).

3.4. Seasonal variation of FHg concentrations

We collected additional samples between October 2018 and July 2019 at four sites within the salt marsh estuary (TW1, TW4, and TW7) and the Parker river freshwater site (PR) to assess seasonality during the whole sample period from October 2018 to September 2020 (Figs. S8 and S9). Seasonal patterns at the fresh water site (PR) showed a high degree of variability both of FHg and THg with no distinct seasonal patterns and no statistically significant correlations to river discharge. Ocean water samples (OW1) showed little temporal variation for FHg. All three locations within the salt marsh estuary (TW1, 4 and 7) showed seasonal patterns of FHg with generally highest concentrations in summer (July) and lowest concentrations in winter (December to February). Spring and fall months generally were transition months with FHg concentrations in spring gradually increasing towards the summer maxima and concentrations in fall declining towards the winter minima. However, these patterns were not fully consistent across the sampling sites, with exceptions including low May concentration at TW1, high concentrations in October at TW4, and high concentration in October at TW7. Another notable pattern is that seasonal amplitude of FHg was by far strongest in the upper marsh estuary (e.g., from 0.28 ng L^{-1} to 2.25 ng L^{-1} at site TW1) compared to a smaller amplitude in the middle/lower marsh (e.g., 0.45 ng L^{-1} to 1.30 ng L^{-1} at site TW4). THg concentration showed generally more variability and among the highest concentrations in July and August, although exceptions to these patterns occurred such as high concentrations also observed in February. In summary, seasonal patterns show higher FHg during the warm season which is consistent with Fig. 2 showing strongest concentration enhancements in estuarine water of the upper marsh.

3.5. Annual and seasonal mass balance estimation

Annual riverine Hg mass fluxes can be quantified by multiplying riverine Hg concentrations (i.e., FEM) with observed seasonal river discharges. Similarly, multiplication of Hg concentration enhancements in estuarine water (i.e., AEM - FEM) provides quantification of additional internal estuarine Hg sources (Schiebel et al., 2018). Monthly river water flows from the Parker River from 1946 to 2020 (USGS Water Data for the Nation, 2020) were used and separated into river discharge for the four meteorological seasons. In Table 2, we show calculated seasonal Hg mass fluxes for FHg and THg by multiplying concentrations with approximate season river discharge, including riverine exports, internal estuary sources, and combined export to the ocean. Note that we did not include analogue mass balance estimates for FMeHg, DOC,

Table 2
Estimated seasonal and annual FHg and THg mass fluxes based on river discharges and calculated FEM and AEM Hg concentration estimates.

Category	Aug-19	Feb-20	May-20	Sep-20
	Summer	Winter	Spring	Fall
Hg Species	FHg			
Riverine Discharge (L sec^{-1})	844	1266	2381	500
Hg Conc. Of AEM (ng L^{-1} - mean and 95% confidence interval	2.1 (1.5–2.6)	1.6 (1.5–1.6)	1.3 (1.1–1.4)	1.3 (0.1–2.4)
Hg Conc. Of FEM (ng L^{-1})	0.9	1.0	0.7	0.7
Diff Hg Conc.: AEM – FEM (ng L^{-1})	1.2	0.5	0.6	0.6
Hg Conc. Of River (ng L^{-1})	1.0	1.0	0.7	0.7
Seasonal[a] Riverine Hg mass flow (g $season^{-1}$)	6.8	9.9	13.2	2.8
Seasonal internal Hg mass mobilization (g $season^{-1}$)	7.7	5.3	11.0	2.3
Annual riverine Hg mass flow (g yr^{-1})	33			
Annual internal mass Hg mass mobilization (g yr^{-1})	26			
Combined annual mass flow (ocean export) (g yr^{-1})	59			
Hg Species	THg			
Riverine Discharge (L sec^{-1})	844	1266	2381	500
Hg Conc. Of AEM (ng L^{-1} – mean and 95% confidence interval)	11.5 (5.4–17.6)	10.7 (8.8–12.6)	4.8 (3.3. to 6.3)	4.8 (2.4–11.9)
Hg Conc. Of FEM (ng L^{-1})	0.85	0.77	1.39	0.53
Diff Hg Conc.: AEM – FEM (ng L^{-1})	10.66	9.94	3.40	4.23
Hg Conc. Of River (ng L^{-1})	0.86	0.76	1.38	0.52
Seasonal Riverine Hg mass flow (g $season^{-1}$)	5.7	7.6	25.9	2.0
Seasonal internal Hg mass mobilization (g $season^{-1}$)	70.9	99.2	63.8	16.7
Annual riverine Hg mass flow (g yr^{-1})	41			
Annual internal mass Hg mass mobilization (g yr^{-1})	251			
Combined annual mass flow (ocean export) (g yr^{-1})	292			

[a] Northern meteorological seasons: Spring - March 1st to May 31st, Summer - Jun 1st to August 31st, Fall - September 1st to November 30th, and Winter - December 1st to February 28th.

and TOC since linear regression analyses generally showed no significant differences between FEM and AEM for these species. For FHg, riverine export of FHg is estimated at 33 g yr^{-1} and an additional 26 g yr^{-1} (range of 18–44 g yr^{-1}) is mobilized from within the salt marsh estuary, for a total annual FHg export to the ocean of about 59 g yr^{-1}. Approximately 44% of the total annual FHg ocean export is attributable to a source within the estuary. Calculated annual riverine export of THg is estimated at 41 g yr^{-1} and an additional 251 g yr^{-1} (range of 125–377 g yr^{-1}) was mobilized from within the salt marsh estuary, for a total annual watershed export of THg of 292 g yr^{-1} (Table 2). For THg, approximately 86% of the total annual export to the ocean is attributable to internal THg sources within the estuary. Seasonally, lowest riverine FHg and THg fluxes occurred in fall while highest riverine FHg and THg occurred in spring, largely driven by respective seasonal river discharge flows.

4. Discussion

4.1. Transect patterns of inorganic total and filtered Hg across the tidal salt marsh

Our results show a range of Hg concentrations in estuarine water of this salt marsh from 0.22 to 1.56 ng L^{-1} for FHg and 0.29 to 14.07 ng L^{-1} for THg. Tidal marsh aqueous THg concentrations were at the low end of a wide range of THg concentrations reported from other salt marshes, while FHg concentrations were in similar magnitude (Table S4). For example, across eight salt marsh estuaries from Connecticut to the Gulf of Maine along the U.S. east coast, FHg concentrations were between 0.24 and 0.71 ng L^{-1} and THg concentrations were between 0.85 and 46.2 ng L^{-1} (Chen et al., 2014). Another study reported Hg data from six un-contaminated U.S. east coast salt marsh estuaries with a range of 0.25 and 3.95 ng L^{-1} for FHg and 2.22 and 366.2 ng L^{-1} for THg concentrations, and concentrations from three contaminated estuaries were substantially higher (up to 3443 ng L^{-1} for THg and up to 11.9 ng L^{-1} for FHg) (Seelen et al., 2020). Further studies also reported FHg concentrations from 0.75 to 29.7 ng L^{-1} in a salt marsh estuary of northeastern US and THg from 1.18 to 31.1 ng L^{-1} (Balcom et al., 2015) and FHg between 0.18 and 0.77 ng L^{-1} in a Seine River salt marsh estuary in France (Laurier et al., 2003) (Table S4).

Concentrations of FHg and THg in estuarine water of the upper marsh were statistically enhanced compared to upstream riverine Hg concentrations in the Parker River (Fig. 2). Within the estuary, both FHg and THg consistently decreased from the upper marsh to the middle marshes and were lowest in the lower marsh estuary, with statistically significant differences between the three sections. Near-coastal ocean water showed lowest Hg concentrations, similar to low ocean Hg concentrations reported by others (Gworek et al., 2016; Mason et al., 2012; Lamborg et al., 2002). The observation that upper marsh samples were consistently higher in Hg concentrations than freshwater and ocean water is indicative of internal sources of FHg and THg within the salt marsh estuary. In fact, two-endmember mixing models as described by Officer (1979) consistently showed FHg and THg to be enhanced compared to conservative ocean–freshwater mixing lines across the entire salt marsh estuary, with strongest enrichments observed in the upper marsh. Internal sinks and sources of elements in estuaries normally manifest themselves by curvilinear patterns of concentrations versus salinity, and highest enhancements (or drawdowns) would be expected in middle marshes (i.e., convex distribution patterns) (Schiebel et al., 2018; Officer, 1979; Boyle et al., 1974). Hg concentrations in our study, however, did not follow curvilinear patterns but instead increased linearly from the lower to the upper marsh. Such linear behaviors have previously been reported for POC and conductivity in this salt marsh estuary also (Hopkinson et al., 2018). Possible reasons for these patterns include that sources are unevenly distributed across the estuary or that slow turnover and mixing times of estuarine water resulting in non-equilibrium mixing conditions. Also, groundwater Hg inputs could be another possible and uneven source of Hg to estuarine water, which was not accounted for in this study.

Previous studies provide indications of both sources and sinks of Hg present in salt marshes depending on the system, season, and chemical Hg species (Mitchell et al., 2012; Hung and Chmura, 2006). In the Chesapeake Bay in Maryland, USA, a study measured detailed concentration dynamics over ebb and flow tidal cycles in salt marsh channels and showed higher concentrations of PHg and THg in flood tides compared to ebb tides, suggesting Hg import (i.e., sinks) into the salt marsh (Mitchell et al., 2012). Patterns were reversed for FHg indicating export of FHg from the salt marsh to the estuarine water. However, because the PHg sink exceeded the FHg source, the Chesapeake salt

marsh overall served as a net Hg sink dominated by particulate Hg trapping. Reasons that may explain differences to our observations include that the Chesapeake study represented a small salt marsh of 3 ha with a small tidal range (about 0.3 m), while our study occurred at large scales covering 4000 ha of salt marshes with a large tidal amplitudes of 2.5 m (Hopkinson et al., 2018), so that differences may be related to spatial heterogeneity, tidal range, different source/sink footprints, and possibly different sediment dynamics (see below). A study in the Bay of Fundy in Canada estimated salt marsh Hg sinks or sources by temporally constraining accumulation rates of Hg within sediments (Hung and Chmura, 2006). Over a 5-year period, the study estimated strong Hg accumulation rates in surface sediments between 0.1 and 1.1 mg Hg m^{-2} and the authors concluded that part of this accumulation may have been related to Hg sinks via sediment accumulation from watershed imports (Hung and Chmura, 2006).

4.2. Potential internal sources of Hg enhancements in estuarine water

Terrestrial runoff via riverine export often is regarded as the main source of Hg to estuaries, with Hg subsequently being exported to the coastal oceans (Cesário et al., 2018; Mason et al., 2012; Pan and Wang, 2012). Rivers include watershed Hg from atmospheric deposition, geogenic sources and anthropogenic industrial and domestic inputs (Kocman et al., 2017; Pan and Wang, 2012). River discharge of Hg, which globally has been estimated at 27 ± 13 Mmol yr^{-1} (Amos et al., 2014), is strongly bound to particles with lesser amounts transported via dissolved organic carbon (DOC) (Chen et al., 2014; Amos et al., 2014). Across 10 salt marsh estuaries in the northeastern U.S., Seelen et al. (2020) concluded that the dominant sources both of THg and FHg are upstream watershed export as indicated by strong correlations with DOC concentrations (Pearson's correlation coefficients, r, of 0.7 between FHg and DOC across non-contaminated estuaries), similar to observations by others (Stoken et al., 2016; Bergamaschi et al., 2012). As discussed above, in our study, aqueous concentrations of the Parker River could not explain estuarine water Hg concentrations, while other tributaries (e.g., Ipswich, Little, and Mull rivers) are much smaller or drain only into the low lower marsh (Fig. 1). Although we also observed linear correlations between FHg and DOC (r value of 0.75) across samples, detailed analysis of Hg to DOC ratios showed ratios in estuarine water samples to be significantly enhanced compared to that of freshwater-ocean water mixing line, and we found highest Hg to DOC ratios in the upper marshes indicative of internal Hg enrichments in the intertidal marsh (Fig. S5). Mass balance estimates (section 4.4) suggest internal Hg sources to dominate over import from upstream watershed in our study.

A potential internal source of Hg in this estuary includes mobilization from sediments. Seelen et al. (2020) showed that correlations between sediment and water column Hg concentrations ($r = 0.72$) across 10 salt marsh estuaries (including three highly contaminated sites) are indicative of substantial sediment remobilization and release of legacy Hg from contaminated sediments to the water column, a correlation which was largely lost when considering only uncontaminated sites ($r = 0.28$). Contaminated estuaries in the study of Seelen et al. (2020) had known industrial point sources and showed very high sediment Hg concentrations (average 5235 μg kg^{-1}, median: 796 μg kg^{-1}, compared to uncontaminated sediments averaging 82 μg kg^{-1} [median: 44 μg kg^{-1}]). Other studies also reported high Hg concentrations in contaminated coastal sediments (e.g., Minamata Bay in Japan, 86–3460 μg kg^{-1}, Li et al., 2009; Northeastern coast of U.S., 221–2962 μg kg^{-1}, Kwon et al., 2014; California Coast, 87–3870 μg kg^{-1}, Davydov et al., 2018; Tagus Estuary in Portugal, 0.30–126 μg g^{-1}, Cesário et al., 2017b). Preliminary sediment Hg concentrations measured in our study, however, showed low Hg concentrations (average of 23 μg kg^{-1}) and no evidence of legacy sediment contamination. However, a previous sediment mass balance study (Hopkinson et al., 2018) reported that sediments in this salt marsh may in parts derive from ocean import and suggested potential origin from the nearby Merrimack River, a major New England river that drains 5 km north of the Plum Island sound and may recirculate sediments into the Plum Island Sound during flood tides (Zhao et al., 2010). It is possible that Merrimack River sediment sources possibly contain some level of industrial Hg pollution from a legacy of industrial activity along the nearby Merrimack river (Evers et al., 2007; Ceasar et al., 1976) and may have contribute legacy Hg to this estuary as has been hypothesized earlier (Lane et al., 2011; Evers et al., 2007). However, we did not systematically sample sediments across the entire transect and more detailed sediments studies are needed to clarify the influence of sediments Hg contributions.

Another potential internal Hg source is lateral transport of Hg from salt marsh soils to the water column. Origins of Hg to salt marsh soils would include a combination of atmospheric wet and dry deposition processes (Zhang et al., 2019; Zhou et al., 2021). Wet deposition is estimated around 5.2 μg m^{-2} yr^{-1} in the region based on National Atmospheric Deposition Program mercury network maps of interpolated wet deposition (NADP, 2017). A nearby coastal study on the south-western tip of Cape Cod by Engle et al. (2010) reported much lower wet deposition of 2.9 μg m^{-2} yr^{-1}, along with dry estimates of 1.2 μg m^{-2} yr^{-1} based on multiple resistance models, which included reactive gaseous Hg (RGM) of 1.0 μg m^{-2} yr^{-1} and fine particulate Hg of 0.14 μg m^{-2} yr^{-1}. Atmospheric deposition directly to the estuary, hence, may be an important source of Hg given the high ratio of estuary to total watershed surface area (60 km^2; or 28% of the total watershed area of 212 km^2) (Hopkinson et al., 2018). A further deposition process includes assimilation of atmospheric Hg by vegetation, which subsequently is transferred to soils and often dominates as a source in upland ecosystems (Obrist et al., 2016; Obrist et al., 2011). Atmospheric gaseous Hg(0) uptake by plants and subsequent litterfall, throughfall, and plant die-off generally serves as the most important source of Hg in upland sites accounting for 70–90% of total ecosystem Hg deposition (Wang et al., 2016; Obrist et al., 2017; Jiskra et al., 2015; Demers et al., 2013; Butcher et al., 1992). Salt marsh vegetation, however, may also emit Hg (0) to the atmosphere, as reported in contaminated marshes (Canário et al., 2017; Cesário et al., 2021). Also, a study by Lamborg et al. (2019) were able to explain salt marsh Hg accumulation rates with current wet add dry deposition loadings without a need for an additional sources such as from plant uptake. Hence, the potential role of wetland plants may be more complex than in upland ecosystems and we suggest to clarify the potential contributions of Hg by salt marsh vegetation, which cover an estimated two thirds of the estuarine surface area (Hopkinson et al., 2018; Raymond and Hopkinson, 2003). Salt marsh ecosystems show high annual aboveground productivity averaging 1.05 kg biomass m^{-2} yr^{-1} (Morris and Sundberg, 2020), thereby matching the productivity of upland ecosystems (De Oliveira et al., 2019).

If plants indeed take up substantial amount of atmospheric Hg, it is possible that they drive high salt marsh soil Hg concentrations and subsequent transfer to estuarine water, similar to the "outwelling" hypothesis known to occur for organic carbon (Kalber, 1959). Many studies have shown that salt marshes laterally export organic carbon that is assimilated by plants, driven by salt marshes excess production of autochthonous carbon (i.e., produced via photosynthesis) over what is degraded and stored within the system, resulting in net carbon export to the coastal ocean. A review of salt marsh studies (Tobias and Neubauer, 2009) showed that most salt marshes are considered net exporters of DOC (e.g., in 11 of 13 studies) with export rates ranging from 15 to 328 g m^{-2} $year^{-1}$. For particulate organic carbon (POC), data are more variable with some salt marshes showing net import (e.g., in five of eight studies, range of 3–140 g C m^{-2} $year^{-1}$) while others show net export (in three other studies; export rates ranging of 11–128 g C m^{-2} $year^{-1}$) (Tobias and Neubauer, 2009). We measured Hg concentrations in soils under salt marshes vegetation and found particularly high Hg concentrations of 200 ± 225 μg kg^{-1} (median 141 μg kg^{-1}) in salt marsh soils, with a high degree of variability due to strong depth patterns. On average, soil Hg concentrations were about an order of magnitude larger

than those of tidal flat sediments (23 ± 2 μg kg^{-1}). Hence, a potential origin of Hg to estuarine water may stem from salt marsh soils enriched in Hg. Raymond and Hopkinson (2003) showed that half of DOC exported from the Plum Island Sound to the ocean originated from salt marsh soils and that based $\Delta^{14}C$ values, internal DOC sources (i.e., from salt marshes) were of modern origin which was preferentially mobilized over older carbon sequestered deeper in soils. Lateral transfer of Hg from salt marsh soils to estuarine water also could explain that largest Hg enrichment are observed in the upper marsh which has the highest salt marsh to water surface area ratios (e.g., >10:1, as opposed to 1:1 in the lower marsh) (Hopkinson et al., 2018) and upper marshes may dominate Hg mobilization in this estuary.

4.3. Transect patterns of filtered MeHg

Our estuarine water analyses showed filtered MeHg concentrations (FMeHg) in estuarine water (range of 0.010–0.160 ng L^{-1}) similar to results from previous salt marsh studies (Table S4). For example, FMeHg concentrations in the Chesapeake Bay estuary showed a range of 0.001–0.640 ng L^{-1} (Mitchell et al., 2012), and Chen el al. (2014) showed FMeHg concentrations across eight salt marsh estuaries along the U.S. East Coast between 0.001 and 0.009 ng L^{-1}. Balcom et al. (2015) reported generally lower concentrations (range from 0.002 to 0.090 ng L^{-1}) as did Laurier et al. (2003) (from 0.008 to 0.020 ng L^{-1}). A wider range, and in parts higher concentrations, of FMeHg was reported across six non-contaminated salt marsh estuaries along the U.S. East Coast by Seelen et al. (2020) with concentrations from 0.002 to 1.148 ng L^{-1}. Seelen also reported much higher estuarine water concentrations in sites affected by known point-source contaminations (range of 0.024–1.491 ng L^{-1}), and the study from Cesário et al. (2018) measured even higher FMeHg concentrations, up to 6.419 ng L^{-1}, in the water column of Tagus estuary, Portugal, near an Hg contaminated salt marsh area. The Hg methylation process, adding a methyl-group to inorganic Hg^{II} species (Fitzgerald et al., 2007), is favored under reducing conditions such as in wetlands and sediments (Chen et al., 2012; Driscoll et al., 2013; Wang et al., 2020) and is driven by anaerobic microbes that contain methylating *hgcAB* genes (Fitzgerald et al., 2007; Hsu-Kim et al., 2018). Cesário et al. (2018) found MeHg remobilization from sediments to the water column in the Tagus estuary in Portugal leading to strong correlations between sediment biogeochemistry and water column MeHg concentrations.

Unlike FHg and THg, FMeHg concentrations were statistically highest in fresh water and decreased statistically from the upper to the lower marshes with lowest concentrations observed in the near-coastal ocean. The patterns suggest that fresh watershed inputs of MeHg dominate as a source of MeHg in this estuary, similar to studies that show MeHg sources in coastal ecosystems to be largely derived from watershed transport (Chen et al., 2014; Fitzgerald et al., 2007). About 5% of total riverine Hg discharged to open ocean is generally found in MeHg form (Mason et al., 2012) and strong correlations between MeHg and DOC are generally indicative of watershed-driven sources in estuaries (Seelen et al., 2020). Such correlations were also found in our study for two of our three sampling dates (r-value between FMeHg and DOC of 0.81 in February and 0.83 in September 2020). Others also proposed estuarine MeHg sources to partially derive from ocean import of MeHg formed in the offshore ocean (Chen et al., 2014; Fitzgerald et al., 2007).

A two-endmember mixing model of FMeHg showed that FMeHg concentrations in salt marsh estuarine water were lower than the conservative linear mixing line both in February and May 2020 (Fig. 5a and b), but high variability of concentrations in September 2020 data precluded detection of clear trends at that date (Fig. 5c). Our data hence suggest no observable internal MeHg sources and even potential losses of MeHg in the estuarine water of this estuary. In contrast, Mitchell et al. (2012) and Gilmour et al. (2018) previously showed salt marsh soils to be potential hotspots of methylation and subsequent MeHg export to estuarine water upon ebb tides. Seelen et al. (2020), however, reported water column MeHg to be poorly correlated to sediment concentrations and suggested that water column MeHg were not driven by underlying sediment inorganic Hg or MeHg concentrations. Preliminary analyses of MeHg concentrations of both intertidal sediments and soils under salt marsh vegetation in our estuary showed generally low MeHg concentrations (sediment concentrations of 0.9 ± 0.6 μg kg^{-1}; soil concentrations of 1.2 ± 2.1 μg kg^{-1}) indicating that salt marsh soils were not enriched in MeHg compared to sediments.

High rates of MeHg demethylation may be a potential reason for MeHg losses in the estuarine water column. Factors influencing both methylation and demethylation include temperature, organic matter, amount of available Hg, redox potential, microbial activities, and others (Bravo et al., 2017; Cesário et al., 2017a; Chen et al., 2018), and their respective controls in estuaries are complex. Hg methylation rates generally are stimulated by warmer temperature (Benoit et al., 2003) while demethylation shows lower temperature dependency (Hudelson et al., 2020). We did not address the temporal or spatial patterns of MeHg production and demethylation patterns in this system to be able to explain potential MeHg losses in estuarine water further.

4.4. Mass balance considerations

Based on mass balance estimate across the four sampling dates, we suggest that total Hg in estuarine water of the salt marsh estuary was dominated by internal Hg sources and exceeded riverine sources by a factor of 2 to almost 15. Filtered Hg generally was dominated by riverine sources in three of the four sampling dates, while internal estuarine sources dominated in August. Extrapolated on an annual basis, we estimate internal estuarine sources of total Hg are around six times larger than riverine sources, while internal sources of filtered Hg account for 81% of riverine inputs. An implication of these mass balance estimates is that riverine export of Hg to the ocean is enhanced by internal salt marsh sources of Hg (THg: from 41 g yr^{-1} to 292 g yr^{-1}; FHg: from 33 to 59 g yr^{-1}) and that internal sources account for 86% and 44% of annual export, respectively, albeit with considerable uncertainty ranges (Table 2). We attribute a strong impact of the tidal estuary on aqueous Hg concentrations to a high ratio of estuary to total watershed area ratio, along with low river water flow (Hopkinson et al., 2018; Raymond and Hopkinson, 2003; Weinstein and Connors, 2001). Possible sources include direct atmospheric deposition of Hg along with potential vegetation uptake of Hg in an estuary where vegetation covers two thirds of the estuary surface area. Additionally, groundwater input not accounted for could be an additional source of Hg (Lamborg et al., 2019). For filtered Hg, mass contributions of internal sources (about 44% of total) are higher than the estuarine surface area to total watershed area (about 28%), suggesting a higher yield of Hg in estuarine areas compared to the wateshed. For THg, a six times larger internal source in the estuary compared to riverine contributions greatly exceed the respective surface area representations.

While water mass balance calculations indicate the estuary to serve as a net source of Hg to the coastal ocean, back-of-the envelope calculations of atmospheric deposition show that it is much leass clear to what degree these marshes currently act as sinks for atmospheric Hg deposition. A study at a nearby site on Cape Cod (Engle et al., 2010) estimated atmospheric Hg deposition in this coastal region of 4.1 μg m^{-2} yr^{-1} (wet deposition: 2.9 μg m^{-2} yr^{-1}; GOM depositon: 1.0 μg m^{-2} yr^{-1}; PHg depositon 0.14 μg m^{-2} yr^{-1}). Scaling this deposition to a salt marsh area of 60 km^2 would yield an estimated depositon of 246 g yr^{-1}. Using higher estimated of wet deposition based on interpolated data by the NADP program in the region (about ~5.2 μg m^{-2} yr^{-1}) (NADP, 2017) along with Engle et al.'s dry deposition estimates would yield a higher atmopsheric flux of about 384 g yr^{-1}, which is possibly further enhanced by elemental Hg(0) uptake by vegetation not accounted for. In comparison, we estimate annual estuarine export of THg of 292 g yr^{-1} and much smaller export of FHg (26 g yr^{-1}). It hence seems that salt marshes currently have relatively similar atmopsheric depositon in comparison

to tidal export, or alternatively act as sinks sequestering atmospheric Hg in excess of tidal export. A net sequestration of Hg would be in support of high Hg accumulation in salt marsh soils which suggest they have acted as substantial ecosystem Hg sinks sequestering Hg either from the atmosphere or watershed inputs. A concern is that disturbances and sea level rise may lead to deteriation of salt marsh ecosystems and increased bank and soil losses with associated mobilization of carbon, sediments, and nutrients (Deegan et al., 2012; Hopkinson et al., 2018), potentially also leading to strong mobilization of Hg currently stored in salt marsh soils.

5. Conclusions

This transect study investigating estuarine Hg dynamics in a large salt marsh estuary in New England indicated strong internal sources of FHg and THg in an estuary. Estuarine water Hg concentrations were consistently highest in upper marsh tidal water and strongly enhanced across estuarine water compared to upstream freshwater and ocean water. Two-endmember mixing models showed concentrations of FHg and THg to be enhanced to conservative mixing lines of river and ocean waters. Patterns of Hg to DOC ratios and seasonal patterns were consistent with Hg enhancements in estuarine water samples. Mass balance calculation indicate that internal sources of FHg and THg account for 44% and 86% of combined annual Hg riverine export, respectively. Unlike FHg and THg, our data show no corresponding enhancement, and even some seasonal losses, of FMeHg in the estuarine water of this estuary. FMeHg concentrations were dominated by fresh water concentrations and decreased gradually from the upper to the lower marshes tidal water, with lowest concentrations observed in the near-coastal ocean.

Possible reasons for internal estuarine sources of inorganic Hg include mobilization and remobilization of Hg from tidal sediments and soils under salt marsh vegetation. Salt marsh soils in particular showed high Hg concentrations an order of magnitude higher than concentrations in tidal flat sediments, and may in parts originate from Hg assumiliation by vegetation. Ongoing research is focusing on the spatial and depth distributions of Hg in sediments and salt marshes of this estuary and a more comprehensive understanding of atmospheric deposition processes including the role of salt marsh vegetation to further constrain the origins of inorganic Hg sources in this tidal salt marsh system.

Credit author statement

Ting Wang: Writing - Original Draft, Writing - Review & Editing, Data Curation, Formal analysis, Validation, Software, Visualization, Investigation, Methodology, Conceptualization, Project administration. Daniel Obrist: Funding acquisition, Supervision, Writing - Review & Editing, Resources, Methodology, Conceptualization, Data Curation, Software, Investigation, Visualization, Project administration.

Declaration of competing interest

The authors declare that they have no known competing financial interests or personal relationships that could have appeared to influence the work reported in this paper.

Acknowledgments

We thank Jun Zhou and Emmay Daly for help with water sampling and laboratory analysis of initial sediment and soil mercury samples. We thank Nancy Pau and the Parker River National Wildlife Refuge for sampling permits and acces. We thank Inke Forbrich, Anne Giblin and other researchers from the Plum Island Ecosystem Long-Term Ecological Research project for support and information about the estuary. We thank thesis committee members Celia Chen from Dartmouth and James Heiss from the UMass Lowell and anonymous reviewers for valuable comments and guidance throughout this research. Funding was provided by awards from the U.S. National Science Foundation Division of Environmental Biology (Award Number: 2027038) and Division of Atmospheric and Geospace Sciences (Award Number:1848212).

Appendix A. Supplementary data

Supplementary data to this article can be found online at https://doi.org/10.1016/j.envpol.2021.118657.

References

Amos, H.M., Jacob, D.J., Kocman, D., Horowitz, H.M., Zhang, Y., Dutkiewicz, S., Horvat, M., Corbitt, E.S., Krabbenhoft, D.P., Sunderland, E.M., 2014. Global biogeochemical implications of mercury discharges from rivers and sediment burial. Environ. Sci. Technol. 48, 9514–9522. https://doi.org/10.1021/es502134t.

Balcom, P.H., Schartup, A.T., Mason, R.P., Chen, C.Y., 2015. Sources of water column methylmercury across multiple estuaries in the Northeast U.S. Mar. Chem. 177, 721–730. https://doi.org/10.1016/j.marchem.2015.10.012.

Benoit, J.M., Gilmour, C.C., Heyes, A., Mason, R.P.L., C, M, 2003. Geochemical and Biological Controls over Methylmercury Production and Degradation in Aquatic Ecosystems. American Chemical Society. https://doi.org/10.1021/bk-2003-0835.ch019.

Bergamaschi, B.A., Krabbenhoft, D.P., Aiken, G.R., Patino, E., Rumbold, D.G., Orem, W. H., 2012. Tidally driven export of dissolved organic carbon, total mercury, and methylmercury from a mangrove-dominated estuary. Environ. Sci. Technol. 46, 1371–1378. https://doi.org/10.1021/es2029137.

Boyle, E., Collier, R., Dengler, A.T., Edmond, J.M., NG, A.C., Stallard, R.F., 1974. On the chemical mass-balance in estuaries. Geochem. Cosmochim. Acta 38, 1719–1728. https://doi.org/10.1016/0016-7037(74)90188-4.

Bravo, A.G., Bouchet, S., Tolu, J., Björn, E., Mateos-Rivera, A., Bertilsson, S., 2017. Molecular composition of organic matter controls methylmercury formation in boreal lakes. Nat. Commun. 8, 1–9. https://doi.org/10.1038/ncomms14255.

Butcher, S.S., Charlson, R.J., Orians, G.H., Wolfe, G.V., 1992. Global biogeochemical cycles. Glob. Biogeochem. Cycles 1475–1492. https://doi.org/10.1111/1462-2920.13280.

Canário, J., Caetano, M., Vale, C., Cesário, R., 2007. Evidence for elevated production of methylmercury in salt marshes. Environ. Sci. Technol. 41, 7376–7382. https://doi.org/10.1021/es071078j.

Canário, J., Poissant, L., Pilote, M., Caetano, M., Hintelmann, H., O'Driscoll, N.J., 2017. Salt-marsh plants as potential sources of Hg0 into the atmosphere. Atmos. Environ. 152, 458–464. https://doi.org/10.1016/j.atmosenv.2017.01.011.

Ceasar, J., Collier, R., Edmond, J., Frey, F., Matisoff, G., Ng, A., Stallard, R., 1976. Chemical dynamics of a polluted watershed, the Merrimack river in northern New England. Environ. Sci. Technol. 10, 697–704. https://doi.org/10.1021/es60118a006.

Cesário, R., Hintelmann, H., Mendes, R., Eckey, K., Dimock, B., Araújo, B., Mota, A.M., Canário, J., 2017a. Evaluation of mercury methylation and methylmercury demethylation rates in vegetated and non-vegetated saltmarsh sediments from two Portuguese estuaries. Environ. Pollut. 226, 297–307. https://doi.org/10.1016/j.envpol.2017.03.075.

Cesário, R., Hintelmann, H., O'Driscoll, N.J., Monteiro, C.E., Caetano, M., Nogueira, M., Mota, A.M., Canário, J., 2017b. Biogeochemical cycle of mercury and methylmercury in two highly contaminated areas of Tagus estuary (Portugal). Water Air Soil Pollut. 228 https://doi.org/10.1007/s11270-017-3442-1.

Cesário, R., Monteiro, C.E., Nogueira, M., O'Driscoll, N.J., Caetano, M., Hintelmann, H., Mota, A.M., Canário, J., 2016. Mercury and methylmercury dynamics in sediments on a protected area of Tagus estuary (Portugal). Water Air Soil Pollut. 227 https://doi.org/10.1007/s11270-016-3179-2.

Cesário, R., Mota, A.M., Caetano, M., Nogueira, M., Canário, J., 2018. Mercury and methylmercury transport and fate in the water column of Tagus estuary (Portugal). Mar. Pollut. Bull. 127, 235–250. https://doi.org/10.1016/j.marpolbul.2017.11.066.

Cesário, R., O'Driscoll, N.J., Justino, S., Wilson, C.E., Monteiro, C.E., Zilhão, H., Canário, J., 2021. Air concentrations of gaseous elemental mercury and vegetation-air fluxes within saltmarshes of the Tagus Estuary, Portugal. Atmosphere 12 (228). https://doi.org/10.3390/atmos12020228.

Chen, C.Y., Borsuk, M.E., Bugge, D.M., Hollweg, T., Balcom, P.H., Ward, D.M., Williams, J., Mason, R.P., 2014. Benthic and pelagic pathways of methylmercury bioaccumulation in estuarine food webs of the Northeast United States. PLoS ONE 9. https://doi.org/10.1371/journal.pone.0089305.

Chen, C.Y., Driscoll, C.T., Eagles-Smith, C.A., Eckley, C.S., Gay, D.A., Hsu-Kim, H., Keane, S.E., Kirk, J.L., Mason, R.P., Obrist, D., Selin, H., Selin, N.E., Thompson, M.R., 2018. A critical time for mercury science to inform global policy. Environ. Sci. Technol. 52, 9556–9561. https://doi.org/10.1021/acs.est.8b02286.

Chen, C.Y., Driscoll, C.T., Kamman, N.C., 2012. Mercury Hotspots in Freshwater Ecosystems: Drivers, Processes, and Patterns. Mercury Environ.: Pattern Process 143–166.

Crooks, S., Herr, D., Tamelander, J., Laffoley, D., Vandever, J., 2011. Mitigating climate change through restoration and management of coastal wetlands and near-shore marine ecosystems: challenges and opportunities. In: Environment Department Papers. World Bank, Washington, DC.

Das, R., Bizimis, M., Wilson, A.M., 2013. Tracing mercury seawater vs. atmospheric inputs in a pristine SE USA salt marsh system: mercury isotope evidence. Chem. Geol. 336, 50–61. https://doi.org/10.1016/j.chemgeo.2012.04.035.

Davydov, R., Sokolov, M., Hogland, W., Glinushkin, A., Markaryan, A., 2018. The application of pesticides and mineral fertilizers in agriculture, in: MATEC Web of Conferences. EDP Sciences, p. 11003. https://doi.org/10.1051/matecconf/201824511003.

De Oliveira, C.P., Francelino, M.R., Daher, M., De Araújo, E.J.G., De Souza Sanches, L., De Andrade, K.D.C., De Campos, J.S.N., 2019. Estimation of the aboveground biomass and carbon stocks in open Brazilian Savannah developed on sandy soils. Carbon Bal. Manag. 14, 1–10. https://doi.org/10.1186/s13021-019-0121-0.

Deegan, L.A., Johnson, D.S., Warren, R.S., Peterson, B.J., Fleeger, J.W., Fagherazzi, S., Wollheim, W.M., 2012. Coastal eutrophication as a driver of salt marsh loss. Nature 490, 388–392. https://doi.org/10.1038/nature11533.

Demers, J.D., Blum, J.D., Zak, D.R., 2013. Mercury isotopes in a forested ecosystem: implications for air-surface exchange dynamics and the global mercury cycle. Global Biogeochem. Cycles 27, 222–238. https://doi.org/10.1002/gbc.20021.

Driscoll, C.T., Mason, R.P., Chan, H.M., Jacob, D.J., Pirrone, N., 2013. Mercury as a global pollutant: sources, pathways, and effects. Environ. Sci. Technol. 47, 4967–4983. https://doi.org/10.1021/es305071v.

Engle, M.A., Tate, M.T., Krabbenhoft, D.P., Schauer, J.J., Kolker, A., Shanley, J.B., Bothner, M.H., 2010. Comparison of atmospheric mercury speciation and deposition at nine sites across central and eastern North America. J. Geophys. Res. Atmos. 115 https://doi.org/10.1029/2010JD014064.

Evers, D.C., Han, Y.-J., Driscoll, C.T., Kamman, N.C., Goodale, M.W., Lambert, K.F., Holsen, T.M., Chen, C.Y., Clair, T.A., Butler, T., 2007. Biological mercury hotspots in the northeastern United States and southeastern Canada. Bioscience 57, 29–43. https://doi.org/10.1641/b570107.

Fitzgerald, W.F., Lamborg, C.H., Hammerschmidt, C.R., 2007. Marine biogeochemical cycling of mercury. Chem. Rev. 107, 641–662. https://doi.org/10.1021/cr050353m.

Gedan, K.B., Silliman, B.R., Bertness, M.D., 2009. Centuries of human-driven change in salt marsh ecosystems. Ann. Rev. Mar. Sci. 1, 117–141. https://doi.org/10.1146/annurev.marine.010908.163930.

Gilmour, C., Bell, J.T., Soren, A.B., Georgia, Riedel, Riedel, Gerhardt, Kopec, A.D., Bodaly, R.A., 2018. Distribution and biogeochemical controls on net methylmercury production in Penobscot River marshes and sediment. Sci. Total Environ. 640–641, 555–569. https://doi.org/10.1016/j.scitotenv.2018.05.276.

Gworek, B., Bemowska-Kałabun, O., Kijeńska, M., Wrzosek-Jakubowska, J., 2016. Mercury in marine and oceanic waters—a review. Water Air Soil Pollut. 227 https://doi.org/10.1007/s11270-016-3060-3.

Hopkinson, C.S., Morris, J.T., Fagherazzi, S., Wollheim, W.M., Raymond, P.A., 2018. Lateral marsh edge erosion as a source of sediments for vertical marsh accretion. J. Geophys. Res.: Biogeosciences 123, 2444–2465. https://doi.org/10.1029/2017JG004358.

Howes, B.L., Goehringer, D.D., 1994. Porewater drainage and dissolved organic carbon and nutrient losses through the intertidal creekbanks of a New England salt marsh.

Hsu-Kim, H., Eckley, C.S., Achá, D., Feng, X., Gilmour, C.C., Jonsson, S., Mitchell, C.P.J., 2018. Challenges and opportunities for managing aquatic mercury pollution in altered landscapes. Ambio 47, 141–169. https://doi.org/10.1007/s13280-017-1006-7.

Hudelson, K.E., Drevnick, P.E., Wang, F., Armstrong, D., Fisk, A.T., 2020. Mercury methylation and demethylation potentials in Arctic lake sediments. Chemosphere 248. https://doi.org/10.1016/j.chemosphere.2020.126001, 126001.

Hung, G.A., Chmura, G.L., 2006. Mercury accumulation in surface sediments of salt marshes of the Bay of Fundy. Environ. Pollut. 142, 418–431. https://doi.org/10.1016/j.envpol.2005.10.044.

Jackson, A.K., Evers, D.C., Etterson, M.A., Condon, A.M., Folsom, S.B., Detweiler, J., Schmerfeld, J., Cristol, D.A., 2011. Mercury exposure affects the reproductive success of a free-living terrestrial songbird, the Carolina Wren (Thryothorus Ludovicianus), the auk. https://doi.org/10.1525/auk.2011.11106.

Jiskra, M., Wiederhold, J.G., Skyllberg, U., Kronberg, R.M., Hajdas, I., Kretzschmar, R., 2015. Mercury deposition and Re-emission pathways in boreal forest soils investigated with Hg isotope signatures. Environ. Sci. Technol. 49, 7188–7196. https://doi.org/10.1021/acs.est.5b00742.

Kalber, F.J., 1959. A hypothesis on the role of tide-marshes in estuarine productivity. Estuar. Bull. 4, 3.

Kocman, D., Wilson, S.J., Amos, H.M., Telmer, K.H., Steenhuisen, F., Sunderland, E.M., Mason, R.P., Outridge, P., Horvat, M., 2017. Toward an assessment of the global inventory of present-day mercury releases to freshwater environments. Int. J. Environ. Res. Publ. Health 14. https://doi.org/10.3390/ijerph14020138.

Kwon, S.Y., Blum, J.D., Chen, C.Y., Meattey, D.E., Mason, R.P., 2014. Mercury isotope study of sources and exposure pathways of methylmercury in estuarine food webs in the northeastern U.S. Environ. Sci. Technol. 48, 10089–10097. https://doi.org/10.1021/es5020554.

Lamborg, C., Mincer, T., Buchanan, W., Collins, C., Swarr, G., Ganguli, P., Whalen, K., Bothner, M., Valiela, I., 2019. Mercury speciation and retention in a salt marsh undergoing long-term fertilization. Estuarine. Coast. Shelf Sci. 218, 188–196. https://doi.org/10.1016/j.ecss.2018.11.031.

Lamborg, C.H., Fitzgerald, W.F., Damman, A.W.H., Benoit, J.M., Balcom, P.H., Engstrom, D.R., 2002. Modern and historic atmospheric mercury fluxes in both hemispheres: global and regional mercury cycling implications. Global Biogeochem. Cycles 16. https://doi.org/10.1029/2001gb001847, 51–1-51–11.

Lane, O., Adams, E.M., Pau, N., O'Brien, K.M., Regan, K., Farina, M., Schneider-Moran, T., Zarudsky, J., 2020. Long-term monitoring of mercury in adult saltmarsh sparrows breeding in Maine, Massachusetts and New York, USA 2000–2017, Ecotoxicology. Springer US. https://doi.org/10.1007/s10646-020-02180-w.

Lane, O.P., O'Brien, K.M., Evers, D.C., Hodgman, T.P., Major, A., Pau, N., Ducey, M.J., Taylor, R., Perry, D., 2011. Mercury in breeding saltmarsh sparrows (Ammodramus caudacutus caudacutus). Ecotoxicology 20, 1984–1991. https://doi.org/10.1007/s10646-011-0740-z.

Langer, C.S., Fitzgerald, W.F., Visscher, P.T., Vandal, G.M., 2001. Biogeochemical cycling of methylmercury at Barn Island salt marsh. Wetlands Ecology and Management, vol. 9. USA, Stonington, CT, pp. 295–310. https://doi.org/10.1023/A:1011816819369.

Laurier, F.J.G., Cossa, D., Gonzalez, J.L., Breviere, E., Sarazin, G., 2003. Mercury transformations and exchanges in a high turbidity estuary: the role of organic matter and amorphous oxyhydroxides. Geochem. Cosmochim. Acta 67, 3329–3345. https://doi.org/10.1016/S0016-7037(03)00081-4.

Li, P., Feng, X.B., Qiu, G.L., Shang, L.H., Li, Z.G., 2009. Mercury pollution in Asia: a review of the contaminated sites. J. Hazard Mater. 168, 591–601. https://doi.org/10.1016/J.JHAZMAT.2009.03.031.

Lockfield, K.C., Fleeger, J.W., Deegan, L.A., 2013. Mummichog Fundulus heteroclitus responses to long-term, whole-ecosystem nutrient enrichment. Mar. Ecol. Prog. Ser. 492, 211–222. https://doi.org/10.3354/meps10495.

Marques, B., Lillebø, A.I., Pereira, E., Duarte, A.C., 2011. Mercury cycling and sequestration in salt marshes sediments: an ecosystem service provided by Juncus maritimus and Scirpus maritimus. Environ. Pollut. 159, 1869–1876. https://doi.org/10.1016/j.envpol.2011.03.036.

Mason, R.P., Choi, A.L., Fitzgerald, W.F., Hammerschmidt, C.R., Lamborg, C.H., Soerensen, A.L., Sunderland, E.M., 2012. Mercury biogeochemical cycling in the ocean and policy implications. Environ. Res. 119, 101–117. https://doi.org/10.1016/j.envres.2012.03.013.

Mcowen, C.J., Weatherdon, L.V., Van Bochove, J.W., Sullivan, E., Blyth, S., Zockler, C., Stanwell-Smith, D., Kingston, N., Martin, C.S., Spalding, M., Fletcher, S., 2017. A global map of saltmarshes. Biodiversity Data Journal 5. https://doi.org/10.3897/BDJ.5.e11764.

Mitchell, C.P.J., Jordan, T.E., Heyes, A., Gilmour, C.C., 2012. Tidal exchange of total mercury and methylmercury between a salt marsh and a Chesapeake Bay sub-estuary. Biogeochemistry 111, 583–600. https://doi.org/10.1007/s10533-011-9691-y.

Morris, J., Sundberg, K., 2020. Plum Island ecosystems LTER. Aboveground Biomass from Control Plots in a Spartina Patens-Dominated Salt Marsh at Law's Point. Rowley River. https://doi.org/10.6073/pasta/b9ffef60518d362a2b892d9471dba5ba. Plum Island Ecosystem LTER, MA. ver 11., Environmental Data Initiative.

Munson, K.M., Babi, D., Lamborg, C.H., 2014. Determination of monomethylmercury from seawater with ascorbic acid-assisted direct ethylation. Limnol Oceanogr. Methods 12, 1–9. https://doi.org/10.4319/lom.2014.12.1.

NADP, 2017. National atmospheric deposition program, mercury deposition network [WWW document]. http://nadp.slh.wisc.edu/maplib/pdf/mdn/hg_Conc_2017.pdf.

Nixon, S.W., 1980. Between coastal marshes and coastal waters -- A review of twenty years of speculation and research on the role of salt marshes in estuarine productivity and water chemistry. In: Hamilton, P., Macdonald, K.B. (Eds.), Estuarine and Wetland Processes: with Emphasis on Modeling. Springer US, Boston, MA, pp. 437–525. https://doi.org/10.1007/978-1-4757-5177-2_20.

NOAA, 2020. National oceanic and atmospheric administration tide Predictions [WWW document]. https://www.tidesandcurrents.noaa.gov/noaatidepredictions.html?id=8441241.

Obrist, D., Agnan, Y., Jiskra, M., Olson, C.L., Colegrove, D.P., Hueber, J., Moore, C.W., Sonke, J.E., Helmig, D., 2017. Tundra uptake of atmospheric elemental mercury drives Arctic mercury pollution. Nature 547, 201–204. https://doi.org/10.1038/nature22997.

Obrist, D., Johnson, D.W., Lindberg, S.E., Luo, Y., Hararuk, O., Bracho, R., Battles, J.J., Dail, D.B., Edmonds, R.L., Monson, R.K., Ollinger, S.V., Pallardy, S.G., Pregitzer, K.S., Todd, D.E., Monson, O.R.K., Ollinger, S.V., Pallardy, S.G., Pregitzer, K.S., Todd, D.E., 2011. Mercury distribution across 14 U.S. Forests. Part I: spatial patterns of concentrations in biomass, litter, and soils. Environ. Sci. Technol. 45, 3974–3981. https://doi.org/10.1021/es104384m.

Obrist, D., Pearson, C., Webster, J., Kane, T., Lin, C.J., Aiken, G.R., Alpers, C.N., 2016. A synthesis of terrestrial mercury in the western United States: spatial distribution defined by land cover and plant productivity. Sci. Total Environ. 568, 522–535. https://doi.org/10.1016/j.scitotenv.2015.11.104.

Odum, E.P., 1980. The status of three ecosystem-level hypotheses regarding salt marsh estuaries: tidal subsidy, Ooutwelling, and detritus-based food chains. In: Tobias, C., Neubauer, S. (Eds.), Estuarine Perspectives. Elsevier, pp. 485–495. https://doi.org/10.1016/b978-0-12-404060-1.50045-9.

Officer, C.B., 1979. Discussion of the behaviour of nonconservative dissolved constituents in estuaries. Estuar. Coast Mar. Sci. 9, 91–94. https://doi.org/10.1016/0302-3524(79)90009-4.

Pan, K., Wang, W.X., 2012. Trace metal contamination in estuarine and coastal environments in China. Sci. Total Environ. 421–422, 3–16. https://doi.org/10.1016/j.scitotenv.2011.03.013.

Pennings, S.C., Bertness, M.D., 2001. Chapter 11-salt marsh communities, marine community ecology https://doi.org/1605352284.

Pruefer, A., 2007. QuikChem ® method 10-117-07-1-B DETERMINATION OF CHLORIDE BY FLOW INJECTION ANALYSIS COLORMETRY. Latchat instruments.

Raymond, P.A., Hopkinson, C.S., 2003. Ecosystem modulation of dissolved carbon age in a temperate marsh-dominated estuary. Ecosystems 6, 694–705. https://doi.org/10.1007/s10021-002-0213-6.

Schiebel, H.N., Gardner, G.B., Wang, X., Peri, F., Chen, R.F., 2018. Seasonal export of dissolved organic matter from a New England salt marsh. J. Coast Res. 344, 939–954. https://doi.org/10.2112/jcoastres-d-16-00196.1.

Scudder, B.C., Chasar, L.C., Wentz, D.A., Bauch, N.J., Brigham, M.E., Moran, P.W., Krabbenhoft, D.P., 2009. Mercury in fish, bed sediment, and water from streams across the United States, 1998-2005, U.S. Geological Survey Scientific Investigations Report 2009–5109.

Seelen, E.A., Chen, C.Y., Balcom, P.H., Buckman, K.L., Taylor, V.F., Mason, R.P., 2020. Historic contamination alters mercury sources and cycling in temperate estuaries relative to uncontaminated sites. Water Res. 190 https://doi.org/10.1016/j.watres.2020.116684, 116684.

Stoken, O.M., Riscassi, A.L., Scanlon, T.M., 2016. Association of dissolved mercury with dissolved organic carbon in U.S. rivers and streams: the role of watershed soil organic carbon. J. Am. Water Resour. Assoc. 52 (12) https://doi.org/10.1002/2015WR017849.

Tobias, C., Neubauer, S., 2009. Salt marsh biogeochemistry - an overview. In: Perillo, G. M.E., Wolanski, E., Cahoon, D.R., Brinson, M.M. (Eds.), Coastal Wetlands: an Integrated Ecosystem Approach. Elsevier, Amsterdam, the Netherlands, pp. 1–57.

Tzortziou, M., Neale, P.J., Osburn, C.L., Megonigal, J.P., Maie, N., Jaffé, R., 2008. Tidal marshes as a source of optically and chemically distinctive colored dissolved organic matter in the Chesapeake Bay. Limnol. Oceanogr. 53, 148–159. https://doi.org/10.4319/lo.2008.53.1.0148.

UNEP, 2006. Marine and coastal ecosystems and human well-being: a synthesis report based on the findings ofthe millennium ecosystem Assessment. Unep 76pp.

USEPA, 2002. Method 1631, revision E: mercury in water by oxidation, purge and trap, and cold vapor atomic fluorescence spectrometry (Washington, DC).

USEPA, 2001. Method 1630: methyl mercury in water by distillation, aqueous ethylation, purge and trap, and cold vapor atomic spectrometry (Washington, DC).

USGS Water Data for the Nation, 2020.

Wang, T., Driscoll, C.T., Hwang, K., Chandler, D., Montesdeoca, M., 2020. Total and methylmercury concentrations in ground and surface waters in natural and restored freshwater wetlands in northern New York. Ecotoxicology. https://doi.org/10.1007/s10646-019-02155-6.

Wang, X., Bao, Z., Lin, C.J., Yuan, W., Feng, X., 2016. Assessment of global mercury deposition through litterfall. Environ. Sci. Technol. 50, 8548–8557. https://doi.org/10.1021/acs.est.5b06351.

Weinstein, M.J., Connors, S.G., 2001. Parker river watershed water quality assement report.

Weis, J.S., Weis, P., 2004. Metal uptake, transport and release by wetland plant s: implications for phytoremediation and restoration. Environ. Int. 30, 685–700. https://doi.org/10.1016/j.envint.2003.11.002.

Wendt, K., 2001. Determination of Nitrate/Nitrite in surface and wastewaters by flow injection analysis (low flow method). Latchat Instruments. QuikChem® Method 10-107-04-1-J.

Zhang, H., Moffett, K.B., Windham-Myers, L., Gorelick, S.M., 2014. Hydrological controls on methylmercury distribution and flux in a tidal marsh. Environ. Sci. Technol. 48, 6795–6804. https://doi.org/10.1021/es500781g.

Zhang, L., Zhou, P., Cao, S., Zhao, Y., 2019. Atmospheric mercury deposition over the land surfaces and the associated uncertainties in observations and simulations: a critical review. Atmos. Chem. Phys. 19, 15587–15608. https://doi.org/10.5194/acp-19-15587-2019.

Zhao, L., Chen, C., Vallino, J., Hopkinson, C., Beardsley, R.C., Lin, H., Lerczak, J., 2010. Wetland-estuarine-shelf interactions in the Plum Island sound and Merrimack river in the Massachusetts coast. J. Geophys. Res.: Oceans 115, 1–13. https://doi.org/10.1029/2009JC006085.

Zhou, J., Obrist, D., Dastoor, A., Jiskra, M., Ryjkov, A., 2021. Vegetation uptake of mercury and impacts on global cycling. Nat. Rev. Earth Environ. 123456789, 1–16. https://doi.org/10.1038/s43017-021-00146-y.